Characterization of Surface Deformation around Vickers Indents in Monocrystalline Materials

P. PERALTA, R. LEDOUX, R. DICKERSON, M. HAKIK, and P. DICKERSON

The deformation surrounding Vickers indents on copper and $MoSi_2$ monocrystals has been characterized for two orientations of the indenter diagonals using optical, electron, and scanning probe microscopy. The surface topography around the indents was characterized using atomic force microscopy (AFM), whereas orientation imaging microscopy (OIM) was used to map the local crystallographic orientation of the surface surrounding one indent on copper and measure lattice rotations due to plastic strain. The results indicate that sink-in and pile-up behavior depend on in-plane crystallographic orientations rather than the orientation of the indenter. Regions with multiple slip show larger lattice rotations and sink-in, whereas regions with lower slip density have smaller lattice rotations and show pile-ups. Strains outside one indent were obtained from OIM data using kinematical relations for single-crystal plasticity. A von Mises strain of 29 pct next to the middle of indent edge on the surface of the sample was deduced from the analysis. This agrees well with the characteristic strain reported for Vickers indents.

I. INTRODUCTION

INDENTATION tests can provide valuable information from probing small volumes, which provides an easy method to evaluate mechanical properties of metallic thin films and advanced intermetallic materials.[1–10] The examination of the imprint left by a hard indenter and measurements of load and penetration have led to methods to measure elastic properties, yield strength, and even hardening behavior.[1–5,7–11] Sharp indenters also lead to geometrically similar indentation states that result in a characteristic strain around them.[7] These characteristics make sharp indenters quite useful in estimating mechanical properties.

Most models for indentation behavior used to estimate mechanical properties assume isotropic material behavior; however, a small indent in a polycrystalline material is likely to be in a single grain, where the behavior can be highly anisotropic. Indentation has also been used extensively to study mechanical properties of single crystals,[6,9–25] mostly because conventional testing methods are difficult to implement. Single crystals display hardness anisotropy in terms of both the crystallography of the indentation plane and the diagonal orientation in pyramidal indenters.[13–15,21,22] This anisotropy is compounded by variations on the surface deformation as a function of the diagonal orientation with respect to the crystallographic axes of the sample. Both sink-in and pile-up, which are indicative of high and low strain hardening rates, respectively,[7,26] have been observed around Vickers indents on a given plane for two orientations of the indent diagonals.[15] This implies that the true contact area is a function of crystallography, which must be taken into account to measure properties from indentation testing.[7,26]

All these facts suggest that studies in isotropic materials cannot fully account for the actual indentation behavior of anisotropic materials; hence, indentation of anisotropic substrates needs to be studied in more detail to account for effects of elastic and plastic anisotropy. Therefore, monocrystalline specimens were used in this work to understand the effect of slip geometry and crystallography on the mechanics of indentation in anisotropic substrates, with emphasis on the surface deformation modes around the indents.

II. EXPERIMENTAL

Copper and $MoSi_2$ were used, because copper is a model fcc material, whereas $MoSi_2$ provides an interesting contrast, given its tetragonal $C11_b$ structure ($c/a \approx 2.45$) and complex slip behavior.[27] Copper crystals were grown using the Bridgman technique and $MoSi_2$ crystals with a modified Czochralski technique in a Centorr (Nashua, NH) Tri-Arc furnace[28] using the conditions shown in Reference 29. Samples with dimensions $5 \times 5 \times 10$ mm^3 were cut using electrodischarge machining (EDM), with edges parallel to [110], [$\bar{1}$10], and [001], as determined by back-reflection Laue. Copper samples were electropolished in 30 vol pct phosphoric acid and 70 vol pct water at 1 V. $MoSi_2$ samples were polished with 1200-grit SiC, 1-μm diamond paste, and 0.05-μm colloidal silica. Indents were made on the (001) plane for both materials, because it matches the symmetry of the Vickers indenter. Diagonals were aligned with either <110> or <100> directions to study orientation effects on the surface deformation around the indents.

A CSEM (Needham, MA) load-depth sensing indentation machine was used for testing. Loads of 0.02, 5, and 10 N were used for copper, and 0.2 and 10 N for $MoSi_2$. Ten indents were made for each testing condition to ensure reproducibility. One typical indent result was chosen to illustrate the results presented. Low loads indents were less than 1 μm deep, and atomic force microscopy (AFM) was used to obtain the surface topography. Scans for $MoSi_2$ were performed with an Auto Probe (Veeco

P. PERALTA, Assistant Professor, and R. LEDOUX and M. HAKIK, Graduate Students, are with the Department of Mechanical and Aerospace Engineering, Arizona State University, Tempe, AZ 85487. Contact e-mail: pperalta@asu.edu R. DICKERSON and P. DICKERSON, Technical Staff Members, are with Los Alamos National Laboratory, Los Alamos, NM 87545.

This article is based on a presentation in the symposium "Terence E. Mitchell Symposium on the Magic of Materials: Structures and Properties" from the TMS Annual Meeting in San Diego, CA in March 2003.

Metrology Group, Santa Barbara, CA) M5E Scanning Probe Microscopy (SPM) system with a scan range of 100 μm in x and y, and 1.5 μm in z. Copper indents were scanned with a Digital Instruments Nanoscope II (Veeco Metrology Group, Santa Barbara, CA) with a J-head, with similar characteristics to those shown previously. Slip was studied with optical microscopy using Nomarski contrast. In addition, orientation imaging system (OIM) was used to obtain the lattice orientation as a function of position around one of the large copper indents. These studies were carried out using an FEI (Hillsboro, OR) XL-30 scanning electron microscope at 20 kV.

III. RESULTS AND DISCUSSION

A. *Slip Patterns*

The slip patterns around $MoSi_2$ indents for the two diagonal orientations are shown in Figure 1. The shape of the indents, indicative of sink-in or pile-up, and the slip behavior depend on the diagonal orientation. The cracking around indents with <110> diagonals (Figure 1a) affected the slip behavior; hence, the slip pattern in Figure 1(b) was reconstructed by collecting the features that were common among all indents made for this case. The indents had a "pin-cushion" shape, indicating sink-in. Cracking around indents with <100> diagonals (Figure 1(c)) did not affect the slip patterns significantly. These indents were "barrel shaped," characteristic of pile-up, and had slip traces parallel to <100> directions in groups extending along <010> directions, regardless of the diagonal orientation. Traces along <110> directions were also observed beyond the volume of the indents for both orientations. Boldt *et al.*[30] found that {110}<001> and {101}<010> systems were operative for Vickers indents on the (001) plane of $MoSi_2$. They were active regardless of the diagonal orientation, as shown in Figures 1(b) and (d), with slip on {101}<010> extending into the crystal. Traces along <110> correspond to {110}<001> dislocation loops punched out during the indentation. The reader should keep in mind that these systems are not equivalent due to the tetragonality of $MoSi_2$ ($c/a \approx 2.45$).

The indents in copper are shown in Figure 2. The slip lines are parallel to the <110> directions, from slip on the {111}<110> systems, as expected. In addition, as was the case for the $MoSi_2$ samples, the indent with diagonals parallel to the <110> directions (Figures 2(a) and (b)) had a pincushion shape, whereas the indent with diagonals along the

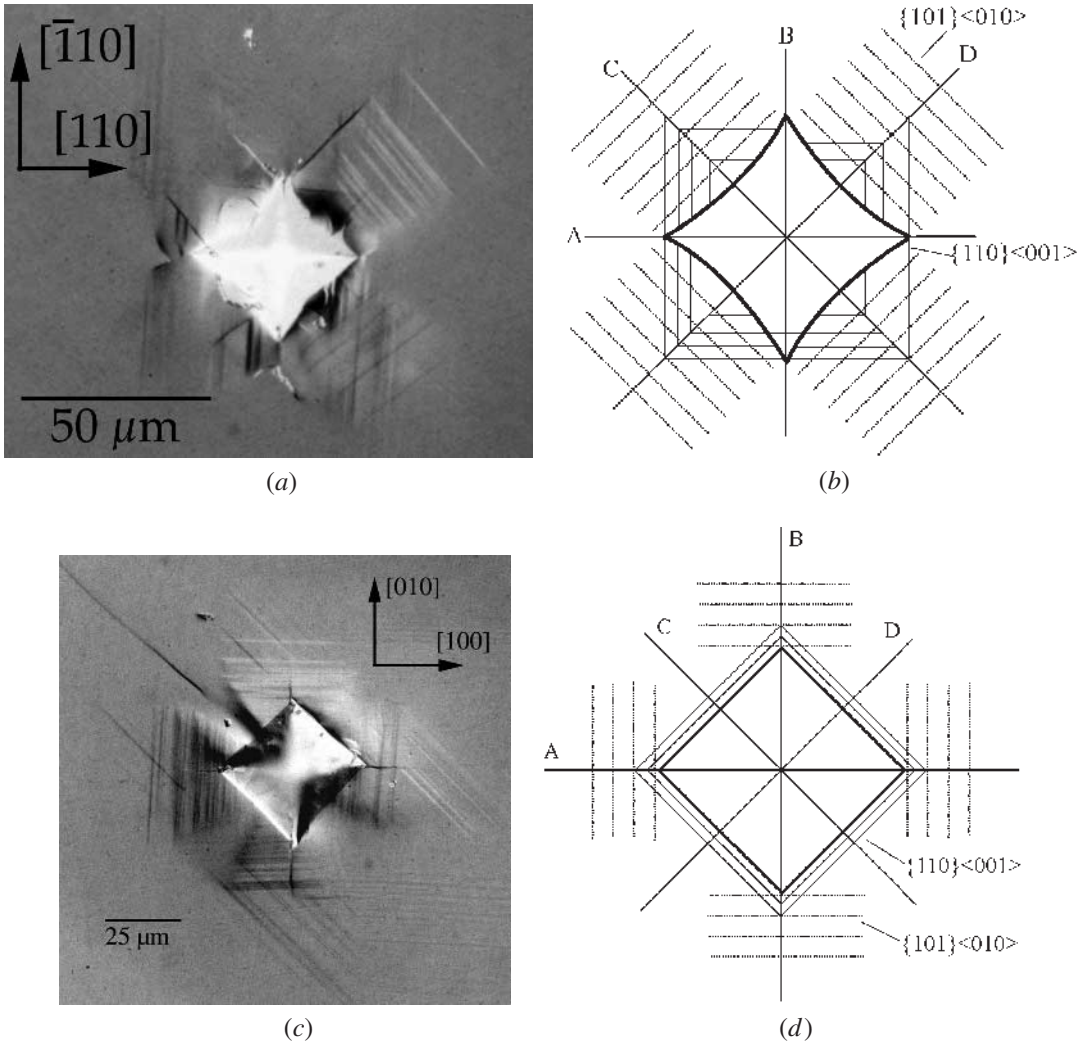

Fig. 1—Indents in $MoSi_2$ at 10 N: (*a*) and (*b*) <110> diagonals; and (*c*) and (*d*) <100> diagonals.

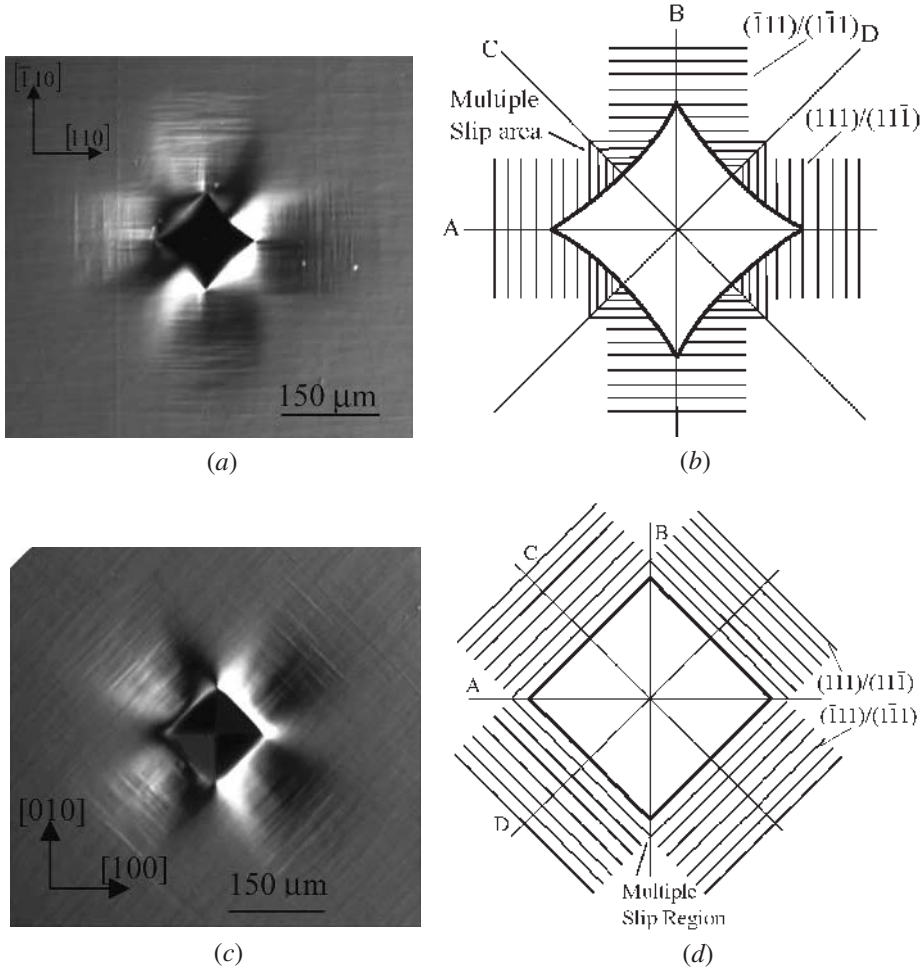

Fig. 2—Indents in copper at 5 N: (*a*) and (*b*) <110> diagonals; and (*c*) and (*d*) <100> diagonals.

<100> directions (Figures 2(c) and (d)) showed barreling along the <110> directions. Note that slip traces parallel to <110> directions formed groups that extended perpendicular to the traces regardless of the diagonal orientation. The intersection of these groups resulted in zones with multiple slip, as indicated in the figures. The resulting surface deformation modes are quantified in Section B using AFM.

B. *Surface Topography*

Height maps for low load indents in $MoSi_2$ are shown in Figure 3. The sink-in around the indents with <110> diagonals can be seen clearly (Figure 3(a)), as well as the square region around the indent where plastic punching takes places.[30] The indents with <100> diagonals (Figure 3(b)) were almost square, but some pile-up was observed at the midsides. Cracking was not found at this load for either case, but the shape of the indents is qualitatively the same as that at larger loads. Line profiles were obtained from the AFM scans to quantify the surface deformation. These profiles were taken along the diagonals and the centers of the indent sides.

The line profiles for a <110>-oriented indent in $MoSi_2$ are shown in Figure 4. The flat portions of the profile traces, corresponding to the facets inside the indent, were fit with straight lines to find the points where the profile separates from the lines. These points define the contact perimeter between the sample and the Vickers indenter, within the error due to elastic unloading. Figure 4(a) indicates that pile-up occurs in <110>-oriented indents at the indent corners. The profile along the indent side is shown in Figure 4(b). A large amount of sink-in is observed, as the departure points are well below the surface of the sample. The sink-in, defined as the vertical distance from the original surface to the departure points, is about 25 pct of the total depth and occurs along <100> directions. Note that there is material pile-up beyond the sink-in. The {110}<001> slip system produces material flow parallel to the indentation direction[30] and is operative near the indent (Figure 4), contributing to the sink-in near the impression. On the other hand, the observed pile-up is believed to occur by slip reversal on the {101}<010> system upon unloading.[30] In addition, this slip system extends into the crystal, as shown in Figure 1(b), to regions where it no longer interacts with {110}<001> slip. This could reduce strain hardening and lead to pile-up. Indentations with <100>-diagonals displayed similar trends regarding sink-in and pile-up. Profiles along the diagonal and the side of a <100> indent are shown in Figure 5. The diagonal profile (Figure 5(a)) shows that sink-in occurs near the impression followed by pile-up; the same was observed in <110>-oriented

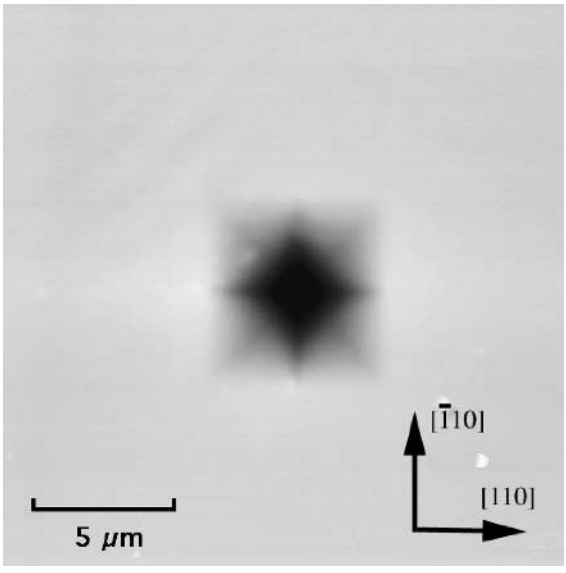

(*a*)

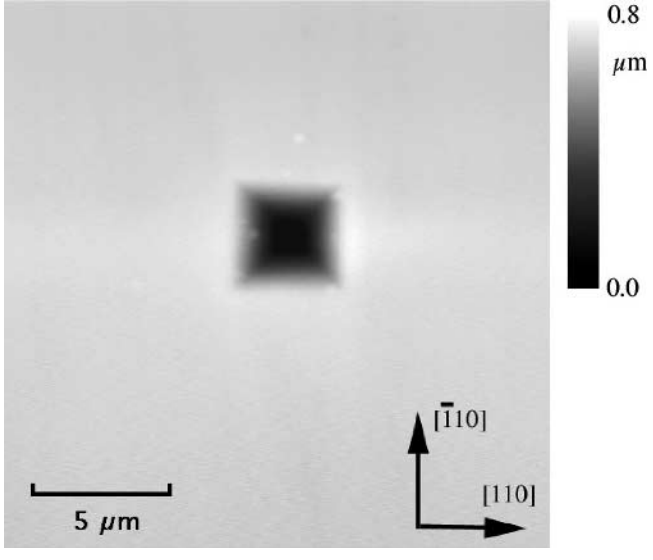

(*b*)

Fig. 3—Height maps for 0.2 N indents in $MoSi_2$: (*a*) <110> diagonals; and (*b*) <100> diagonals.

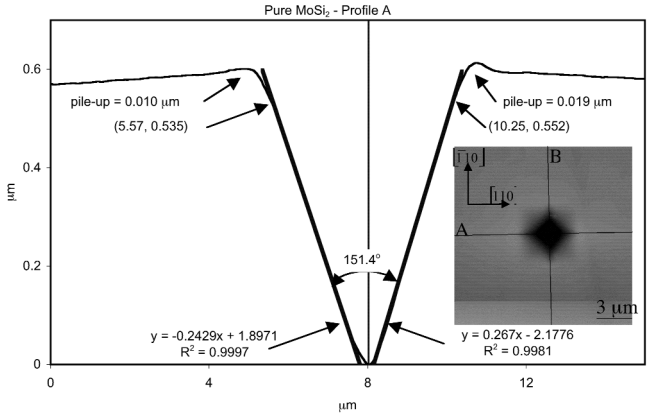

(*a*)

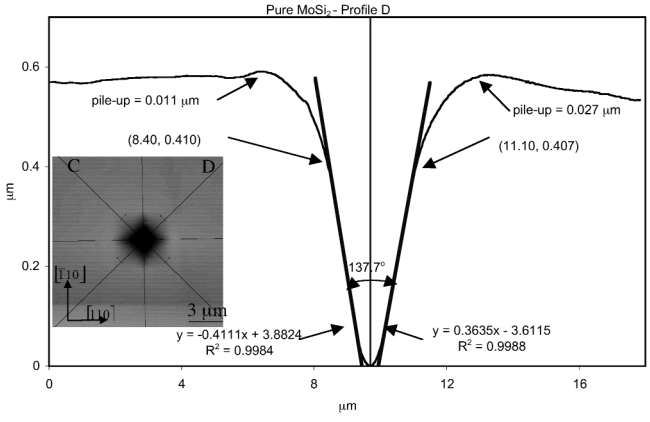

(*b*)

Fig. 4—Line profiles for a 0.2, N <110> indent on $MoSi_2$: (*a*) profile A and (*b*) profile B.

indents along this crystallographic direction, <100> (Figure 4(b)). However, the amount of sink-in is lower in this case, probably because the indenter pushes less material away along its diagonals and conservation of volume would require more material flow along the facets. Line profiles along the midsides of the impression are shown in Figure 5(b) and indicate that pile-up occurred directly outside the edges of the indent facets, as expected.

Surface topography maps for copper indents are shown in Figure 6. These maps showed the same trend of large indents, *i.e.*, <110> indents had sink-in, whereas <100> indents had pile-up. The line profiles along the diagonal and the midface of a <110> indent in copper are shown in Figure 7. Straight lines were also used to find the points of departure, as indicated by arrows. Figure 7(a) shows that pile-up occurred in <110>-oriented indents right outside the corners, as was the case in $MoSi_2$. The pile-up is larger in copper, as expected because slip extended away from the indents along <110> directions, leading to more slip and material flow along these directions than in $MoSi_2$, where the dominant slip traces extended away from the indents along <100> directions. The profile along the midside of the indents is shown in Figure 7(b). Sink-in is observed, as the departure points are below the original surface of the specimen. However, the ratio of sink-in to indent depth is lower than in $MoSi_2$, which may be related to differences in slip interactions for the two materials. In $MoSi_2$, the {101} and {110} slip traces overlap directly along the <100> directions (Figure 1). The interaction of these different slip systems should lead to high strain hardening locally, which correlates with sink-in behavior. Multiple slip also occurs in copper along <100> directions (Figure 2), which can cause higher hardening rates and sink-in. This multiple slip is at the intersection of the slip groups extending along <110> directions, instead of resulting from a direct overlap as in $MoSi_2$, suggesting that the amount of multiple slip and its hardening effect are lower in copper. Nevertheless, there was material pile-up beyond the sink-in, as was the case in $MoSi_2$. This suggests that strain hardening along <100> directions decreased with distance from the indent, probably because the slip interactions also decreased (Figure 2). Pile-up is also likely to result from slip reversal upon unloading as in

$MoSi_2$.[30] Similar behavior was observed in <100>-oriented indents, as shown in Figure 8. The profile along the diagonals (Figure 8(a)) shows that there is sink-in right outside the corners of the indent followed by a small pile-up. This is similar to the profile in <110>-oriented indents for the same crystallographic direction, *i.e.*, <100> (Figure 7(b)). The difference between the two cases is that the amounts of sink-in and subsequent pile-up were higher for the <110>-oriented indents. The <100> direction in <110> indents is along the middle of the indent sides; it is then likely that more material is pushed from under the indenter perpendicular to the indenter facets, leading to more material flow along <100> directions for <110> diagonals and a higher level of sink-in and subsequent pile-up to satisfy conservation of volume. The profiles along the <110> directions for the <100>-oriented diagonals (Figure 8(b)) show a large amount of pile-up. In this case, the profile is along the middle of the indent sides, and more material is being pushed along these directions. This is consistent with the larger pile-up observed as compared to the same crystallographic direction for the <110> indent (Figure 7(a)).

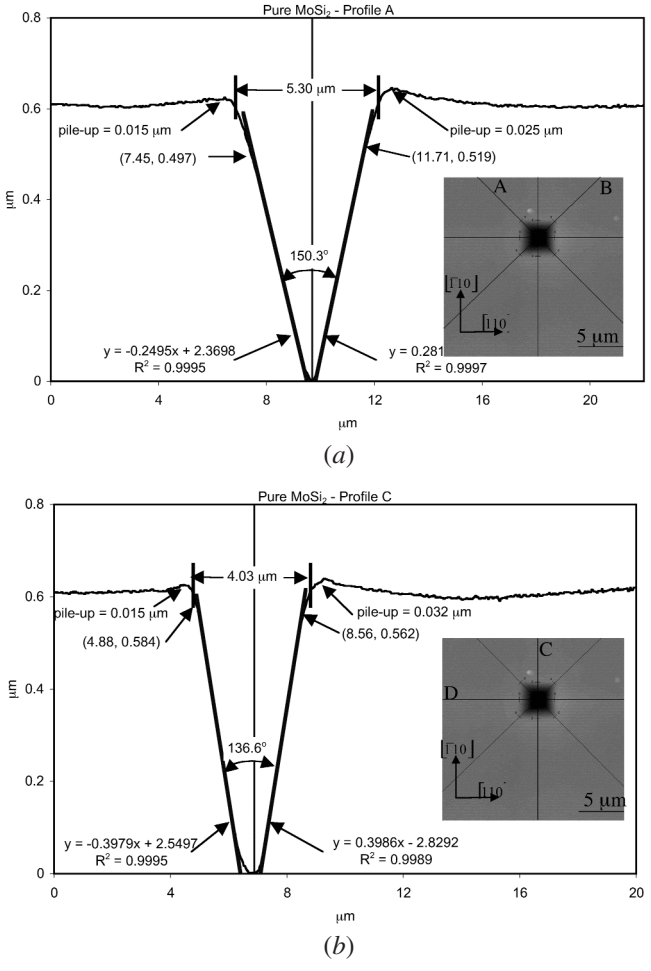

Fig. 5—Line profiles for a 0.2 N, <100> indent on $MoSi_2$: (*a*) profile A and (*b*) profile C.

The AFM data were used to obtain the true contact area of the indents for both materials. This allowed the calculation of the true hardness as a function of diagonal orientation, which is compared to the hardness calculated using the average diagonal length in Table I.

The hardness calculated with the diagonal length does not vary significantly from one diagonal orientation to the other in either material, making it difficult to determine the hardness anisotropy. However, the calculation with the true contact area results in significant differences between the two diagonal orientations, about 44 pct in $MoSi_2$ and 31 pct in copper. This stresses the importance of the surface deformation modes on the determination of hardness in single crystals. The experimental evidence collected indicates that sink-in and pile-up are mainly a function of the crystallographic direction on the indentation plane rather than of the orientation of the indenter diagonals. The two materials showed sink-in followed by pile-up along <100> directions and pile-up along <110> directions. These deformation modes correlated with changes in multiplicity of slip as a function of orientation and distance from the indent. Nevertheless, the slip geometry must also play a role, because

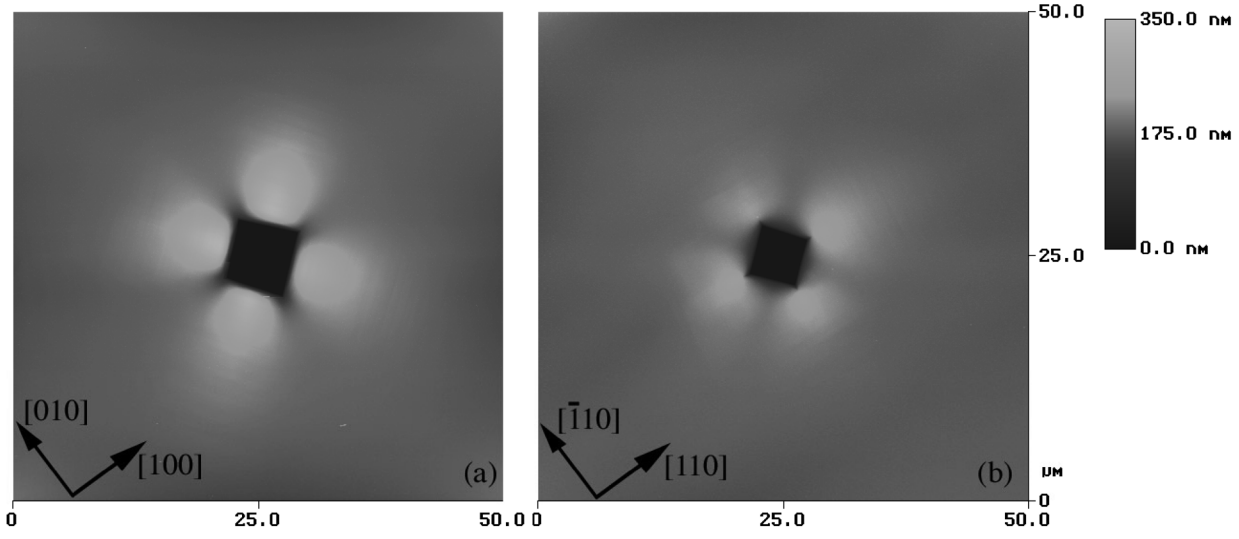

Fig. 6—Height maps for 0.02 N indents in copper: (*a*) <100> diagonals and (*b*) <110> diagonals.

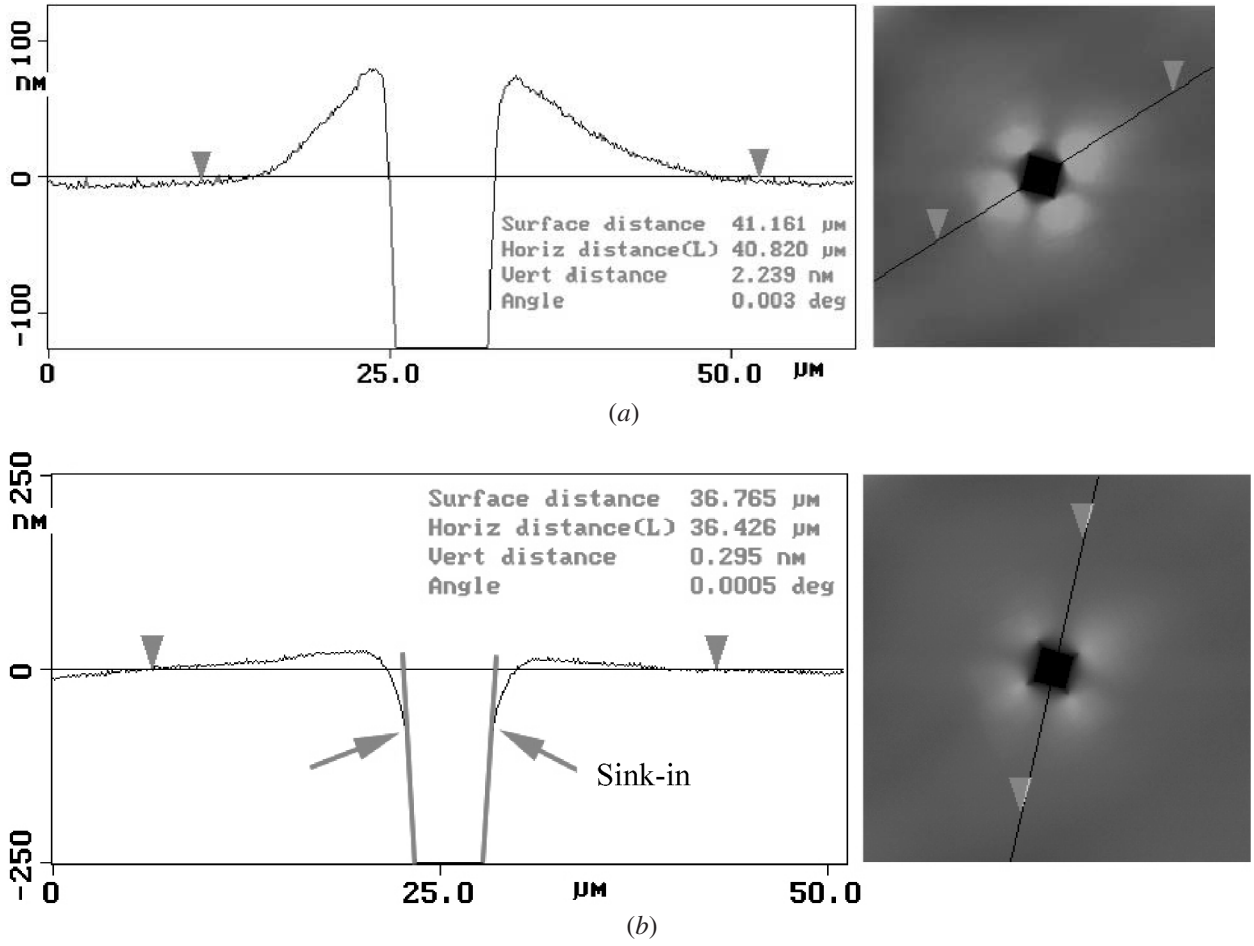

Fig. 7—Profiles for a 0.02 N copper indent with <110> diagonals: (*a*) diagonal and (*b*) midside.

appropriate Burgers vectors are needed to push material into the sample (sink-in) or to take it toward the surface (pile-up). Finite-element models using single-crystal plasticity are being developed to explore this in more detail.

These results also suggest that the mechanism by which the indentation volume is being displaced from under the indenter is a function of the orientation of the indentation plane rather than the orientation of the diagonals. The diagonal orientation seems to bias material flow from under the indenter, with more material being moved perpendicular to the indent facets. However, the multiplicity of slip and slip patterns remained qualitatively the same, producing pile-up and sink-in along <110> and <100> directions, respectively, regardless of the diagonal orientation. In addition, the plastic zone size around copper indents, *i.e.*, the horizontal distance between markers shown in Figures 7 and 8, was similar along the same crystallographic directions for the two diagonal orientations. This suggests that the "details" of the indenter geometry affect the strain fields only in a region adjacent to the indent itself and that the size of the plastic zone in copper depends on the applied load and the crystallography of the slip plane. Similar experiments with spherical indents are being carried out to study this behavior. The size of the plastic zone is an important parameter to calculate yield stresses in polycrystals and single crystals.[31] A method to measure the plastic zone size and an average plastic strain in it as a function of position was developed based on OIM data. This is presented in Section C.

C. *Strain Measurement from Lattice Rotations.*

Indents with <110> diagonals were made in copper with a load of 10 N and then scanned using OIM. Profilometry results indicated that the sink-in region around the indent had an average surface inclination of only 2 deg, which leads to reasonable accuracy for OIM measurements. Indents in $MoSi_2$ had much larger average surface inclinations at the sink-in region, so no attempt was made to study them with OIM. The misorientation angles[32] between the original lattice and the points in a line parallel to the <100> direction, *i.e.*, the midside of the indent, were obtained from OIM data as a function of the distance to the center of the indent. These angles are expected to be accurate to less than 0.5 deg.

The final orientation of the surface normal after the deformation obtained by OIM was used along with the kinematics of slip[33,34] to determine an "equivalent" plastic strain leading to the same final orientation of the tensile axis in a crystal under uniaxial load deformed by double slip. The full details are given in Reference 35, but the main points are shown here for completeness. Under uniaxial tension, the rate of change of a direction l due to slip is given by[33,34]

$$\dot{\mathbf{l}} = \mathbf{L}\mathbf{l} \qquad [1]$$

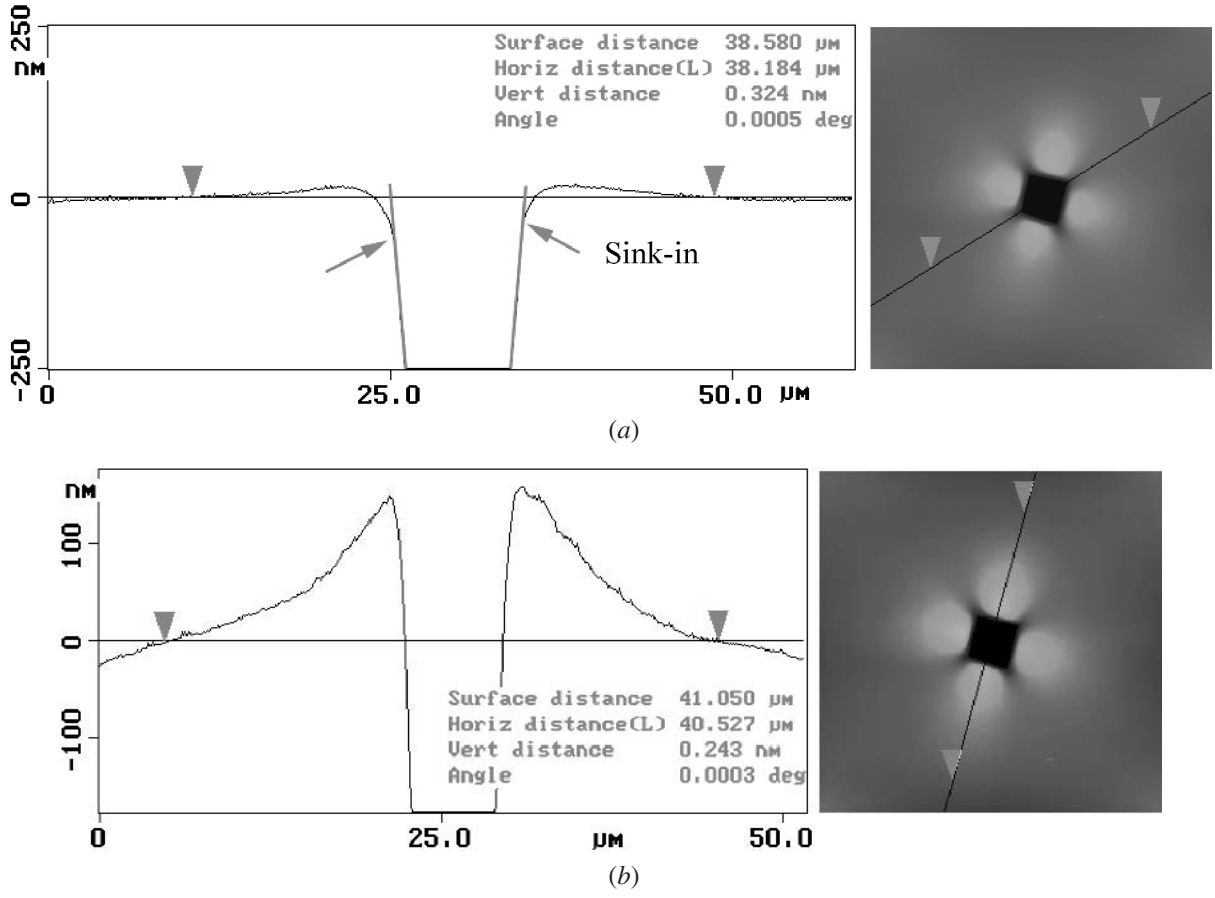

Fig. 8—Profiles for a 0.02 N copper indent with <100> diagonals: (*a*) diagonal and (*b*) midside.

Table I. Hardness (in kg/mm^2) for Low Load Indents in $MoSi_2$ and Cu

	$MoSi_2$		Cu	
Orientation	Diagonals	Contact Area	Diagonals	Contact Area
<110>	1800 ± 100	2000 ± 100	58 ± 2	68 ± 2
<100>	1600 ± 200	1130 ± 50	57 ± 6	47 ± 3

In this equation, **L** is the velocity gradient, which is given by the linear superposition of the contribution of the *m* active slip systems as follows:[33,34]

$$\mathbf{L} = \sum_{\kappa=1}^{m} \dot{\gamma}^{(\kappa)} (\mathbf{b}^{(\kappa)} \otimes \mathbf{n}^{(\kappa)}) \qquad [2]$$

where $\dot{\gamma}^{(\kappa)}$ is the rate of change of the shear strain in slip system κ, $\mathbf{b}^{(\kappa)}$ is the normalized Burgers vector, and $\mathbf{n}^{(\kappa)}$ is the corresponding unit normal to the slip plane.

Equations [1] and [2] lead to a set of differential equations in the components of **l** that can be solved analytically[33,34] if the active systems are known. The OIM data showed that the sample normal rotated toward [$\bar{1}$01], which is a Burgers vector. This resembles proportional double slip straining of a crystal in tension, because the tensile axis rotates toward the dominating slip vector. The other active slip vector was chosen to match the measured rotation of the sample normal. The proportional double slip condition $\dot{\gamma}^{(2)} = \alpha\dot{\gamma}^{(1)}$ leads to the deformation gradient:

$$\mathbf{F} = \mathbf{I} + \gamma^{(1)}\left(\mathbf{b}^{(1)} \otimes \mathbf{n}^{(1)} + \alpha(\mathbf{b}^{(2)} \otimes \mathbf{n}^{(2)})\right) + \alpha(\mathbf{n}^{(2)} \cdot \mathbf{b}^{(1)})\left(\mathbf{b}^{(2)} \otimes \mathbf{n}^{(1)}\right)\frac{(\gamma^{(1)})^2}{2} \qquad [3]$$

The logarithmic strain was computed as $\varepsilon = \ln \mathbf{U}$, where **U** is the Lagrangian stretch tensor given by the polar decomposition $\mathbf{F} = \mathbf{RU}$. The eigenvalues of ε were then used to calculate the von Mises strain ε_{eq}. The shear strain corresponding to each data point along the chosen line was obtained by matching the local normal measured to the one predicted by the analysis. Once the shear strain was obtained, **F** could be calculated at each point and with it the von Mises strain.

The results are plotted in Figure 9. The inset shows the line used for the measurement and the distance *r*. No reliable data could be obtained inside the indent; hence, no points are given for small values of *r*. Note the steep gradient in the misorientation angle close to the indent, which correlates with the strain gradients expected there. The variation of the angle levels off at $r \approx 100$ μm and becomes approximately zero at $r \approx 250$ μm with no significant changes for $r > 250$ μm.

The results suggest that the elastic-plastic boundary should be where the angle no longer changes significantly with distance, *i.e.*, at 250 μm from the center. This results in a ratio of $2r_p/d \approx 2.2$, where r_p is the radius of the plastic zone and

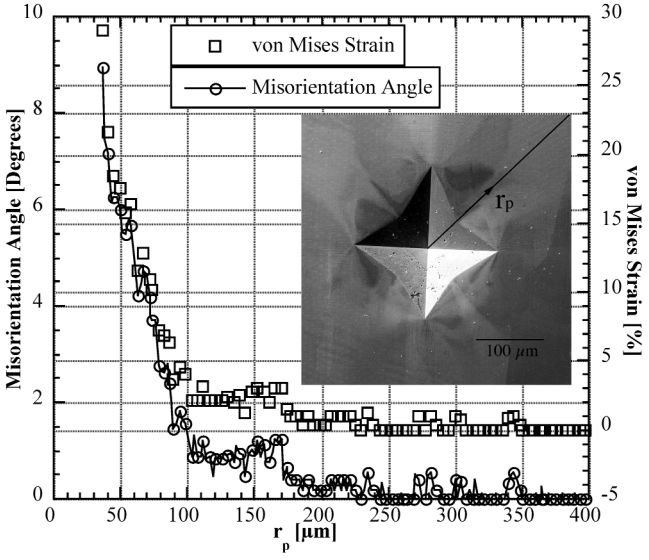

Fig. 9—Misorientation angle and von Mises strain as a function of position.

d is the diagonal length of the indent (227 μm). This is similar to the value of $2r_{pileup}/d$ for the large copper indents shown in Figure 1, where r_{pileup} is the distance from the center of the indent to the top of the pile-up present after the sink-in. This ratio is about 2.3, as measured by profilometry. This indicates that the small pile-up found after the sink-in does not lead to lattice rotations that can be detected with this measurement. It could also be that the strain gradient is so shallow after the sink-in that a longer line was needed to find the end of the plastic zone. However, a correlation was found with an important site from a plasticity point of view. Note that the engineering strain close to the indent is ≈29 pct, which agrees well with the characteristic strain next to Vickers indents reported in the literature.[7,36,37]

IV. CONCLUSIONS

Surface deformation modes related to pile-up and sink-in surrounding a Vickers indent can be present on the same crystallographic plane, even for annealed copper single crystals, for different orientations of the diagonals of the indent. These surface deformation modes are characteristic of a particular crystallographic direction on the plane of indentation; the orientation of the indenter simply changes the amplitude of the deformation, by pushing more material along its facets.

The presence of sink-in and pile-up correlated with different slip multiplicity along particular crystallographic directions. Sink-in was present in regions where at least two slip traces intersected, whereas pile-up was present in regions where just one slip trace was present. The slip geometry is also likely to play a role, but further studies are needed to elucidate this issue. Sink-in and pile-up can be present along the same crystallographic direction. The presence of pile-up after a pronounced sink-in was interpreted in terms of a decrease of the strain hardening in the material as multiplicity of slip decreased as a function of distance from the indent and to possible slip reversal in the volume outside the indent upon withdrawal of the indenter.

The size of the plastic zone obtained from AFM measurements of a Vickers indent showed a strong dependence on crystallographic direction and a weak dependence on indenter orientation. This suggests that material properties derived from measurements of the plastic zone size around indents should not be sensitive to the details of the exact indenter geometry.

Orientation imaging microscopy can provide valuable information on the lattice rotation surrounding an indent and the information on the size of the plastic zone correlates well with optical microscopy estimations of the region where the sink-in outside the indent ends.

A procedure has been developed to obtain an equivalent strain measurement from OIM data based on the final orientation of the sample's normal and the kinematics of plastic deformation via crystallographic slip. The von Mises strain of 29 pct at the edge of the indent shows good agreement with literature reports for the characteristic strain next to a Vickers indent.

ACKNOWLEDGMENTS

This research was supported by the United States National Science Foundation under Grant No. CMS-0084948 and by Los Alamos National Laboratory (MST-8), which provided access to sample preparation, indentation, and OIM facilities.

REFERENCES

1. W.C. Oliver and G.M. Pharr: *J. Mater. Res*., 1992, vol. 7, pp. 1564-83.
2. S. Suresh and A.E. Giannakopoulos: *Acta Mater*., 1998, vol. 46, pp. 5755-67.
3. S. Venkataraman, D.L. Kohlstedt, and W.W. Gerberich: *J. Mater. Res*., 1993, vol. 8, pp. 685-88.
4. T.A. Laursen and J.C. Simo: *J. Mater. Res*., 1992, vol. 7, pp. 618-26.
5. K. Zeng, E. Söderlund, A.E. Giannakopoulos, and D.J. Rowcliffe: *Acta Mater*., 1996, vol. 44, pp. 1127-41.
6. P.H. Boldt, J.D. Embury, and G.C. Weatherly: *Mater. Sci. Eng*., 1992, vol. A155, pp. 251-58.
7. A.E. Giannakopoulos and S. Suresh: *Scripta Mater*., 1999, vol. 40, pp. 1191-98.
8. G.R. Anstis, P. Chantikul, B.R. Lawn, and D.B. Marshall: *J. Am. Cer. Soc*., 1981, vol. 64, pp. 533-38.
9. D.F. Bahr, D.E. Kramer, and W.W. Gerberich: *Acta Mater*., 1998, vol. 46, pp. 3605-3617.
10. W.W. Gerberich, J.C. Nelson, E.T. Lilleodden, P. Anderson, and J.T. Wyrobek: *Acta Mater*., 1996, vol. 44, pp. 3585-98.
11. G.M. Pharr and W.C. Oliver: *J. Mater. Res*., 1989, vol. 4, pp. 94-101.
12. S.A.S. Asif and J.B. Pethica: *Phil. Mag. A*, 1997, vol. 76, pp. 1105-18.
13. C.A. Brookes, J.B. O'Neill, and B.A.W. Redfern: *Proc. R. Soc. London A*, 1971, vol. 322, pp. 73-88.
14. M. Garfinkle and R.G. Garlick: *Trans. TMS-AIME*, 1968, vol. 242, pp. 809-14.
15. S. Kobayashi, T. Okui, and S. Miura: *J. Mater. Sci*., 1993, vol. 28, pp. 3506-12.
16. D. Kramer, H. Huang, M. Kriese, J. Robach, J. Nelson, A. Wright, D. Bahr, and W. Gerberich: *Acta Mater*., 1999, vol. 47, pp. 333-43.
17. S. Harvey, H. Huang, S. Venkataraman, and W.W. Gerberich: *J. Mater. Res*., 1993, vol. 8, pp. 1291-99.
18. S.B. Luyckx, F.R.N. Nabarro, S.-W. Wai, and M.N. James: *Acta Metall. Mater*., 1992, vol. 40, pp. 1623-27.
19. Q. Ma and D.R. Clarke: *J. Mater. Res*., 1995, vol. 10, pp. 853-63.
20. T.F. Page, W.C. Oliver, and C.J. McHargue: *J. Mater. Res*., 1992, vol. 7, pp. 450-73.
21. S.G. Roberts, P.D. Warren, and P.B. Hirsch: *J. Mater. Res*., 1986, vol. 1, pp. 162-75.
22. S.G. Roberts, P.D. Warren, and P.B. Hirsch: *Mater. Sci. Eng*., 1988, vol. A105, pp. 19-28.

23. N.A. Stelmashenko and L.M. Brown: *Phil. Mag. A*, 1996, vol. 74, pp. 1199-206.
24. M.G. Walls, M.M. Chaudhri, and T.B. Tang: *J. Phys. D*, 1992, vol. 25, pp. 500-07.
25. W. Zielinski, H. Huang, S. Venkataraman, and W.W. Gerberich: *Phil. Mag. A*, 1995, vol. 72, pp. 1221-73.
26. J. Alcalá, A.C. Barone, and M. Anglada: *Acta Mater.*, 2000, vol. 48, pp. 3451-64.
27. S.A. Maloy, A.H. Heuer, J.J. Lewandowski, and T.E. Mitchell: *Acta Metall. Mater.*, 1992, vol. 40, pp. 3159-65.
28. T.B. Reed and E.R. Pollard: *J. Cryst. Growth*, 1968, vol. 2, pp. 243-47.
29. S.A. Maloy, T.E. Mitchell, and A.H. Heuer: *Acta Metall. Mater.*, 1995, vol. 43, pp. 657-68.
30. P.H. Boldt, G.C. Weatherly, and J.D. Embury: *J. Mater. Res.*, 2000, vol. 15, pp. 1025-32.
31. D.F. Bahr and W.W. Gerberich: *Metall. Mater. Trans. A*, 1996, vol. 27A, pp. 3793-800.
32. U.F. Kocks, C.N. Tomé, and H.-R. Wenk: *Texture and Anisotropy*, Cambridge University Press, Cambridge, United Kingdom, 1998.
33. A.H. Shalaby and K.S. Havner: *J. Mech. Phys. Solids*, 1978, vol. 26, pp. 79-92.
34. K.S. Havner: *J. Mech. Phys. Solids*, 1979, vol. 27, pp. 415-29.
35. P. Peralta and R. Dickerson: unpublished research, Arizona State University, and Los Alamos National Laboratory, respectively, 2003.
36. A.E. Giannakopoulus, P.-L. Larsson, and R. Vestergaard: *Int. J. Solid Struct.*, 1994, vol. 31, pp. 2679-2708.
37. M.M. Chaudhri: *Acta Mater.*, 1998, vol. 46, pp. 3047-56.